ACS Pharmacology & Translational Science

pubs.acs.org/ptsci

Article

# Natural Compounds Inhibit SARS-CoV-2 nsp13 Unwinding and ATPase Enzyme Activities

Angela Corona, Krzysztof Wycisk, Carmine Talarico, Candida Manelfi, Jessica Milia, Rolando Cannalire, Francesca Esposito, Philip Gribbon, Andrea Zaliani, Daniela Iaconis, Andrea R. Beccari, Vincenzo Summa, Marcin Nowotny, and Enzo Tramontano*

Cite This: *ACS Pharmacol. Transl. Sci.* 2022, 5, 226−239

Read Online

ACCESS | Metrics & More | Article Recommendations | Supporting Information

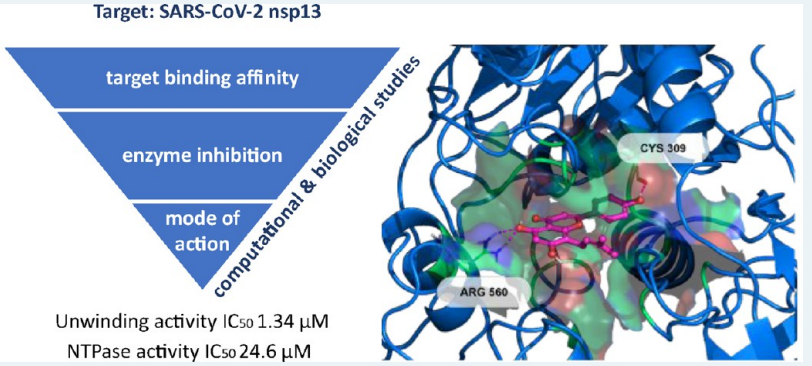


**ABSTRACT:** SARS-CoV-2 infection is still spreading worldwide, and new antiviral therapies are an urgent need to complement the approved vaccine preparations. SARS-CoV-2 nps13 helicase is a validated drug target participating in the viral replication complex and possessing two associated activities: RNA unwinding and 5′-triphosphatase. In the search of SARS-CoV-2 direct antiviral agents, we established biochemical assays for both SARS-CoV-2 nps13-associated enzyme activities and screened both *in silico* and *in vitro* a small in-house library of natural compounds. Myricetin, quercetin, kaempferol, and flavanone were found to inhibit the SARS-CoV-2 nps13 unwinding activity at nanomolar concentrations, while licoflavone C was shown to block both SARS-CoV-2 nps13 activities at micromolar concentrations. Mode of action studies showed that all compounds are nsp13 noncompetitive inhibitors versus ATP, while computational studies suggested that they can bind both nucleotide and 5′-RNA nsp13 binding sites, with licoflavone C showing a unique pattern of interaction with nsp13 amino acid residues. Overall, we report for the first time natural flavonoids as selective inhibitors of SARS-CoV-2 nps13 helicase with low micromolar activity.

**KEYWORDS:** *SARS-CoV-2 inhibition, nsp13, helicase, flavonoid inhibitors, drug development, unwinding inhibition*

Severe acute respiratory syndrome coronavirus-2 (SARS-CoV-2) is the etiological agent of the Coronavirus Disease 2019 (COVID-19), which was initially reported in December 2019 in China and consequently spread in a dramatic pandemic event that has resulted in substantial morbidity and mortality worldwide.[1,2] SARS-CoV-2 is the third highly pathogenic CoV identified so far, following SARS-CoV and Middle East respiratory syndrome coronavirus (MERS-CoV).[3] It is a complex betacoronavirus with a large RNA genome whose transcription and replication are carried out by a viral RNA-dependent RNA polymerase (RdRp, encoded by the non-structural protein 12, nsp12) that has been reported to constitute a complex (holo-RdRp) with the viral cofactors nsp7 and nsp8, the latter with proposed primase or 3′-terminal adenylyltransferase activity.[4−7] In addition, the replication process involves other viral proteins such as the nsp14, providing 3′−5′-exonuclease proofreading and N7-methyltransferase activities, the nsp16 bearing 2′-*O*-methyltransferase activity, involved in the capping machinery, and the nsp13, which provides the RNA helicase and 5′-triphosphatase activities.[7]

The CoVs nsp13 helicase belongs to the 1B (SF1B) helicase superfamily that can unwind DNA or RNA in an NTP-dependent manner with a 5′−3′ polarity.[8,9]. As all SF1 helicases, nsp13 presents two canonical RecA ATPase domains;[10,11] in addition, it contains three domains unique to nidovirus helicases: an N-terminal zinc-binding domain (ZBD), a stalk, and a 1B domain.[8,12−14] While the role of some of these domains

**Received:** November 29, 2021
**Published:** April 1, 2022

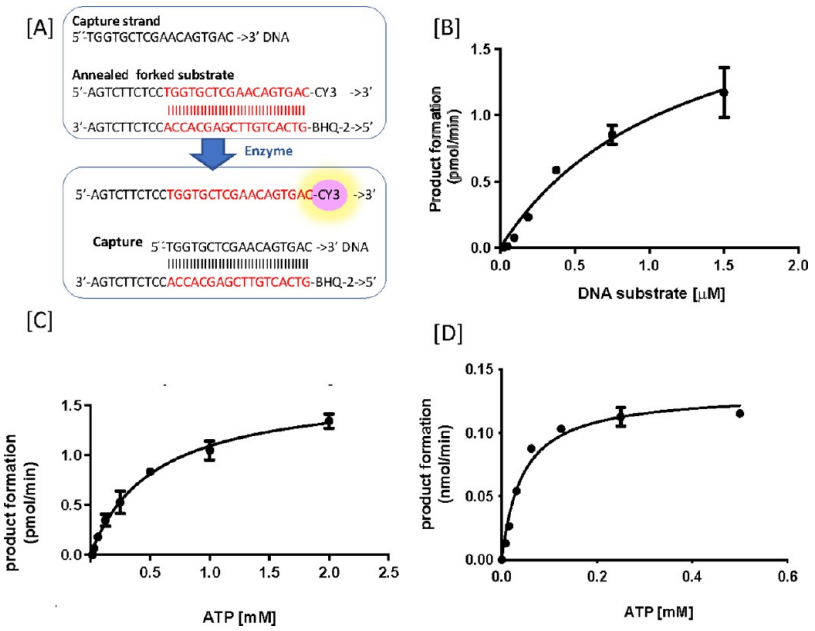


**Figure 1.** SARS-CoV-2 nsp13 kinetics parameters: [A] Scheme of the dsDNA substrate used for the unwinding assay; [B] nsp13 unwinding-associated activity kinetics measured with respect to the DNA substrate; [C] nsp13 unwinding-associated activity kinetics measured with respect to the ATP substrate; [D] nsp13 ATPase-associated activity kinetics measured with respect to the ATP substrate.

is still unclear, the SARS-CoV-2 helicase function is considered to be critical for viral replication, as it has been shown to be essential for other CoVs such as nidovirus equine arteritis virus[15] or $\beta$-CoV murine hepatitis virus.[16] Hence, nsp13 is an essential enzyme for viral replication and a validated target for drug discovery.

Helicases are not a fully explored target for antiviral drug discovery yet; in fact, in the latest years, a few compounds have been reported to inhibit SARS-CoV helicase activity,[17] among them natural flavonoids such as myricetin[18] and baicalein.[19] SARS-CoV-2 nsp13 shows a 99.8% sequence identity with SARS-CoV. Recently a few works explored this promising target and suggested some natural compounds as possible inhibitors such as cepharanthine,[20] active on NTPase activity with an $IC_{50}$ value of 0.4 mM. In the effort of identifying new SARS-CoV-2 inhibitors, *in silico* docking studies were carried out to estimate the theoretical affinity of natural compound libraries with respect to the helicase nsp13, by targeting both orthosteric and allosteric binding sites.[21] Capitalizing from these computational studies and the medical chemistry compound selection performed within the EXSCALATE4COV (E4C) (www.exscalate4cov.eu) project, we tested a small in-house library of natural compounds on the SARS-CoV-2 nsp13-associated activities and identified four flavonoid derivatives that inhibit the nps13-associated unwinding activity in the nanomolar range, without affecting the nsp13-associated ATPase activity. In addition, licoflavone C was found to inhibit both nsp13-associated activities in the micromolar range. Inhibition kinetic studies showed that these compounds are noncompetitive inhibitors against ATP; docking studies suggested their binding to both reported nsp13 binding sites, with differences that could explain their diverse inhibition of the nsp13 enzyme activities.

## RESULTS

**Assay Optimization and Determination of Kinetics Parameters of SARS-CoV-2 nsp13 Enzymatic Activities.** First, we measured the nsp13 double-stranded (ds) nucleic acid unwinding activity using a dsDNA as a substrate, given that it has been previously shown that CoV helicases are equally active in unwinding DNA and RNA substrates.[9] We used a forked dsDNA with ssDNA overhangs at one dsDNA end (Figure 1A). One strand of the duplex was labeled with Cy3, while the other contained a BHQ-2 quencher, so that following nsp13 unwinding activity a strong fluorescent signal of Cy3 could be observed after the removal of the strand with the quencher. An excess of DNA with the same sequence of the one bearing the Cy3 but without the modification was also added to the reaction mixture to prevent reannealing of the displaced strands that would reduce the fluorescent signal. Hence, the reaction measured single turnover events with respect to DNA substrate.[22]

Following optimization of assay conditions, as described in the Materials and Methods section, we determined the kinetic parameters for both substrates, DNA and ATP (Figure 1B,C). Results showed that nsp13 unwinding-associated activity has a $K_m$ value for the dsDNA substrate of 1.22 ± 0.29 $\mu$M, a $K_m$ value for ATP of 0.47 ± 0.06 mM, and a $k_{cat}$ value of 54.25 ± 5.3 $min^{-1}$.

Second, we measured the nsp13 ATPase-associated activity in the absence of any nucleic acid substrate. ATP hydrolysis was quantified using a colorimetric assay detecting the release of Pi produced through the formation of a green complex formed between molybdate/malachite and the liberated orthophosphate. Following optimization of assay conditions, described in the Materials and Methods section, we determined the kinetic parameters for ATP (Figure 1D), obtaining a $K_m$ value for ATP of 0.043 ± 0.012 mM and a $k_{cat}$ value of 211 ± 26 $min^{-1}$.

**Virtual Screening Campaign on SARS-CoV-2 nsp13: Flavonoids among the Best Scored Binders.** Natural polyphenols have been investigated as anti-infective agents against viruses including CoVs. In particular, flavonoids have been previously reported as inhibitors of SARS-CoV and MERS helicases.[17−19] In the context of the EXSCALATE4COV (E4C) (www.exscalate4cov.eu) project, among the screened molecules,


https://doi.org/10.1021/acsptsci.1c00253
ACS Pharmacol. Transl. Sci. 2022, 5, 226−239

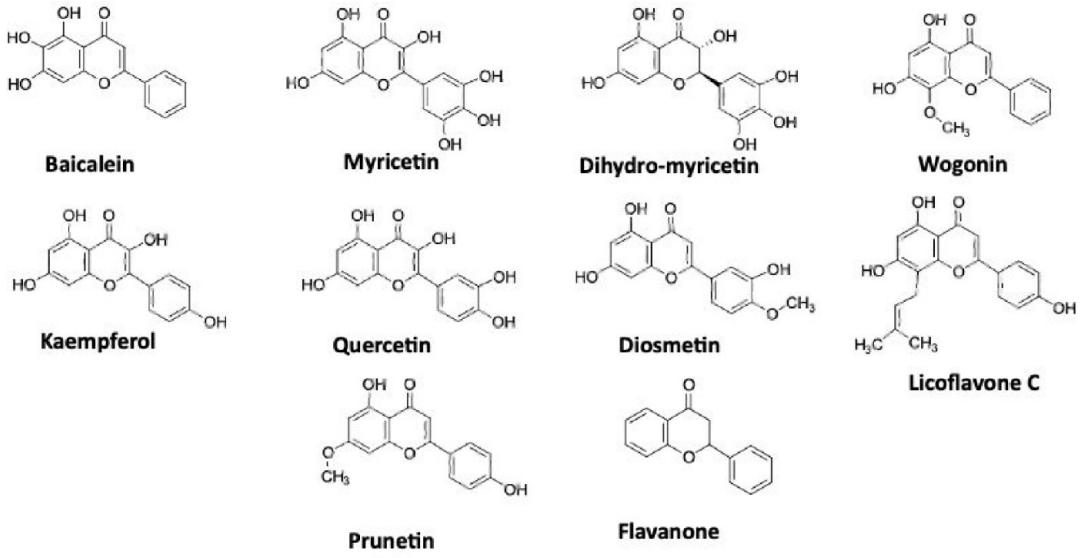


**Figure 2.** Chemical structures of selected natural polyphenols.

flavonoids have emerged as a good candidate to bind nps13 SARS-CoV-2 protein.[21] Hence, 10 commercially available natural polyphenols (Figure 2) were selected as potential binders and further investigated. The nsp13 crystal structures were obtained from the Protein Data Bank (PDB code 6XEZ). Molecular docking simulations were performed with LiGen (Ligand Generator) software on two binding sites, the nucleotide and the 5′-RNA pockets.[21] Table 1 reports the docking score rank obtained on the selected targets. This evidence suggested the ability of this class of compounds to directly bind to nsp13 and possibly inhibit its enzymatic activities.

**Table 1. LiGen Predicted Binding Affinity of the Investigated Compounds to SARS-CoV-2 nsp13 Binding Sites**

| compound | nucleotide site | 5′-RNA site |
|---|---|---|
| licoflavone C | high | high |
| myricetin | medium | high |
| quercetin | medium | high |
| diosmetin | high | low |
| kaempferol | medium | medium |
| baicalein | medium | medium |
| prunetin | low | medium |
| dihydro-myricetin | low | low |
| flavanone | low | low |
| wogonin | low | low |

**In-House Natural Compound Library Screening.** Considering the results of the virtual screening calculation and the literature data on other CoV helicases, the above 10 compounds evaluated *in silico* were tested on the SARS-CoV-2 nsp13 unwinding-associated activity. To explore the molecular space surrounding the ligands, additional compounds were included in the selection: seven structurally related glycosylated flavonoids, three simpler related fragments (ferulic acid, gallic acid, and resveratrol), and quercetin structurally related catechin, present in the in-house library (Figure 3). Compound SSYA10−001, reported to inhibit SARS-CoV nsp13,[23] was used as a positive control, showing an $IC_{50}$ value of 46 nM on SARS-CoV-2 nsp13 unwinding-associated activity.

Out of the 21 tested compounds, 11 inhibited the nsp13-associated unwinding activity, showing $IC_{50}$ values below 30 $\mu$M (Table 2). Notably, the 11 active compounds were all flavonoids, while neither the related flavanol catechin nor other phenolic compounds such as resveratrol, gallic acid, and ferulic acid, were able to inhibit the helicase activity. Within the subset of active flavonoids, four compounds showed $IC_{50}$ values in the nanomolar range (flavanone, kaempferol, myricetin, and quercetin), while three of them were active in the low micromolar range (baicalein, flavanone-7-glucoside, and licoflavone C). The glycosylated compounds were mostly inactive with the sole exception of flavanone-7-glucoside.

All 21 compounds and SSYA10−001 were also tested on the SARS-CoV-2 nsp13-associated ATPase activity (Table 2). Results showed that only licoflavone C was able to inhibit this nsp13 enzyme activity with an $IC_{50}$ value of 24 $\mu$M, thus demonstrating to be a unique dual SARS-CoV-2 nsp13 inhibitor with a ∼20-fold specificity for the nsp13-associated unwinding activity over the nsp13-associated ATPase activity.

Considering the presence of a number of oxygen groups in the flavonoid molecules and the effects of DTT on the flavonoid ability to inhibit other SARS-CoV-2 enzymes,[24] we then asked whether the presence of DTT, and hence the overall reaction oxidation state, could have an impact on the ability of the compounds to inhibit nsp13 functions. Therefore, the most potent compounds, flavanone, kaempferol, myricetin, quercetin, and licoflavone C, were then tested in the presence or absence of 1 mM DTT for the inhibition of nsp13 unwinding-associated activity. Compound SSYA10−001[23] was used as the control (Figure 4). Results showed that kaempferol, myricetin, quercetin, licoflavone C, and SSYA10−001 were equally active in the presence and absence of DTT, indicating either that the reaction oxidation state was not relevant for their inhibition properties or that DTT did not react with compounds. In contrast, the presence of DTT had an effect on flavanone that showed an $IC_{50}$ value of 5.20 ± 1.50 $\mu$M. To complete the evaluation of the DTT effect, we also tested the inhibition of the nsp13 ATPase-associated activity by licoflavone C in the presence or absence of DTT, observing no differences (data not shown).


https://doi.org/10.1021/acsptsci.1c00253
ACS Pharmacol. Transl. Sci. 2022, 5, 226−239

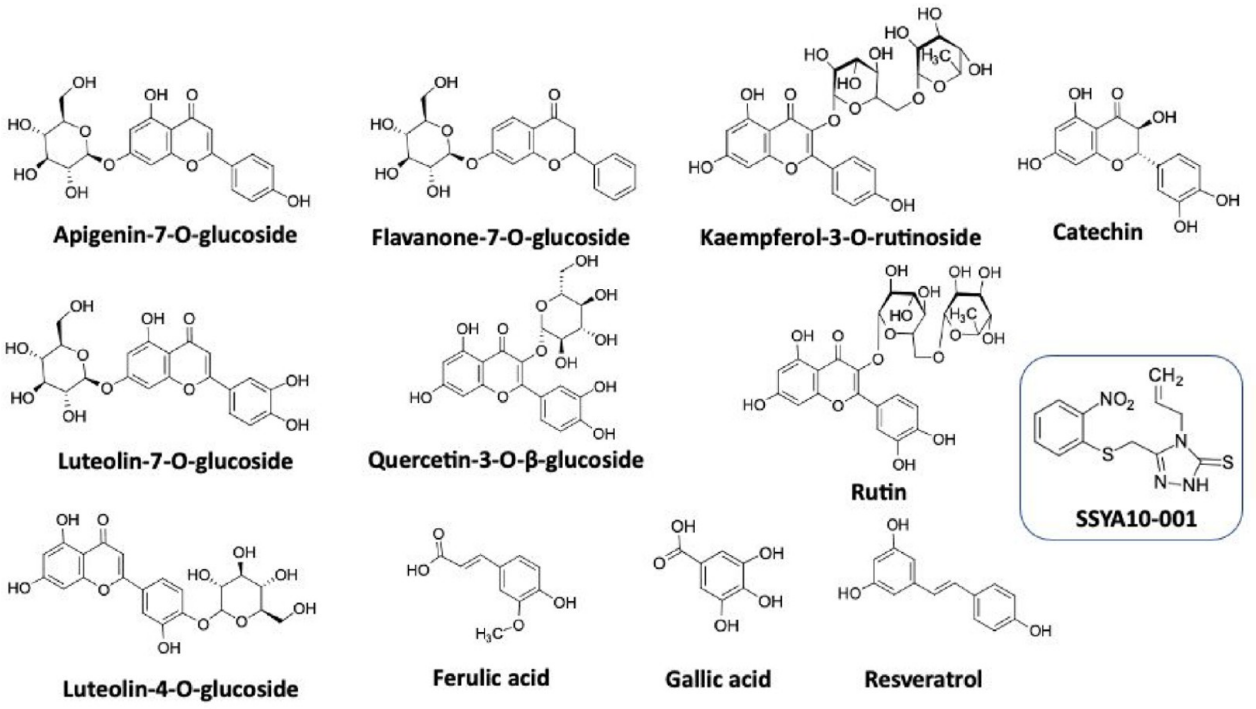


**Figure 3.** Chemical structures of polyphenols.

**Table 2. Inhibition of SARS-CoV-2 nsp13 Helicase-Associated Activities by Natural Compounds**

| | unwinding | unwinding BSA-TCEP | ATPase | ATPase BSA-TCEP-polyrA | SARS-CoV-2 | Vero E6-GFP |
|---|---|---|---|---|---|---|
| compound | $IC_{50}$ ($\mu$M)[a] | $IC_{50}$ ($\mu$M)[a] | $IC_{50}$ ($\mu$M)[b] | $IC_{50}$ ($\mu$M)[b] | $EC_{50}$ ($\mu$M)[c] | $CC_{50}$ ($\mu$M)[d] |
| myricetin | 0.41 ± 0.11 | 19.9 ± 2.3 | >30 (87%)[e] | >30 (97%)[e] | >100 (100%) | >100 (100%) |
| quercetin | 0.53 ± 0.13 | 10.2 ± 1.4 | >30 (86%) | >30 (99%) | >100 (100%) | >100 (100%) |
| flavanone | 0.52 ± 0.24 | 6.48 ± 0.53 | >30 (90%) | >30 (57%) | >100 (100%) | >100 (100%) |
| kaempferol | 0.76 ± 0.16 | 19.0 ± 2.1 | >30 (83%) | >30 (95%) | >100 (100%) | >100 (100%) |
| licoflavone C | 1.34 ± 0.31 | 9.9 ± 0.5 | 24.6 ± 3.8<br>29.0 ± 2.1[g] | 18.3 ± 2.8 | >100 (100%) | >100 (100%) |
| flavanone-7-*O*-glucoside | 2.88 ± 0.88 | 70.6 ± 3.2 | >30 (86%) | >30 (87%)[e] | >100 (100%) | >100 (100%) |
| baicalein | 2.90 ± 1.0 | 10.2 ± 1.1 | >30 (94%) | >30 (100%) | >100 (100%) | >100 (100%) |
| diosmetin | 10.6 ± 5.5 | 57.8 ± 1.2 | >30 (92%) | >30 (100%) | >100 (100%) | >100 (100%) |
| prunetin | 11.5 ± 1.7 | >100 (70%) | >30 (97%) | >30 (91%) | >100 (100%) | >100 (100%) |
| wogonin | 24.9 ± 5.5 | 74.9 ± 8.3 | >30 (95%) | >30 (87%)[e] | nt[f] | nt |
| dihydro-myricetin | 25.6 ± 7.7 | >100 (68%) | >30 (100%) | >30 (96%) | nt | nt |
| catechin | >30 (88%) | nt | >30 (97%) | nt | nt | nt |
| apigenin-7-*O*-glucoside | >30 (100%) | nt | >30 (99%) | nt | nt | nt |
| kaempferol-3-*O*-rutinoside | >30 (71%) | nt | >30 (95%) | nt | nt | nt |
| luteoline-4-*O*-glucoside | >30 (71%) | nt | >30 (89%) | nt | nt | nt |
| luteoline-7-*O*-glucoside | >30 (100%) | nt | >30 (100%) | nt | nt | nt |
| quercetin-3-*O*-*β*-glucoside | >30 (83%) | nt | >30 (100%) | nt | nt | nt |
| rutin | >30 (75%) | nt | >30 (96%) | nt | nt | nt |
| gallic acid | >30 (89%) | nt | >30 (92%) | nt | nt | nt |
| resveratrol | >30 (64%) | nt | >30 (98%) | nt | nt | nt |
| ferulic acid | >30 (64%) | nt | >30 (91%) | nt | nt | nt |
| SSYA10−001 | 0.05 ± 0.02 | 1.73 ± 0.34 | >3 (90%) | >3 (93%) | nt | nt |
| GC376 | >100 | nt | >100 | nt | 0.28 ± 0.04 | >100 (100%) |

[a]Compound concentration required to inhibit the SARS-CoV-2 nsp13-associated unwinding activity by 50%. [b]Compound concentration required to inhibit the SARS-CoV-2 nsp13-associated ATPase activity by 50%. [c]Compound concentration required to reduce the SARS-CoV-2 cytopathic effect in Vero-E6-GFP cells by 50% in the presence of 2 $\mu$M CP100356. [d]Compound concentration required to reduce Vero-E6-GFP cell viability by 50% in the presence of 2 $\mu$M CP100356. [e]Percentage of control measured in the presence of the highest tested compound concentration. [f]Not tested. [g]Determined in the presence of 10 $\mu$g/mL of BSA and 180 $\mu$M TCEP.

In order to exclude the possibility of inhibition by nonspecific aggregator effects, the active compounds were tested on both associated SARS-CoV-2 enzymatic activities in the presence of 10 $\mu$g/mL of BSA and 180 $\mu$M TCEP. First, we assessed enzyme



https://doi.org/10.1021/acsptsci.1c00253
ACS Pharmacol. Transl. Sci. 2022, 5, 226−239

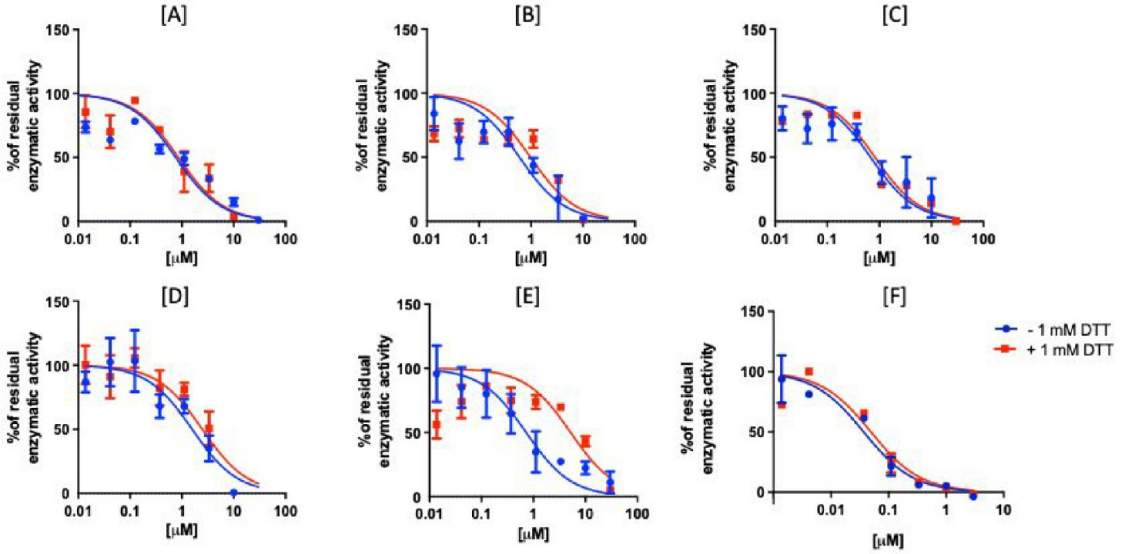


**Figure 4.** Impact of DTT on inhibition of nsp13-associated unwinding activity by flavonoids. [A] Kaempferol; [B] quercetin; [C] myricetin; [D] licoflavone C; [E] flavanone, [F] SSYA10−001.

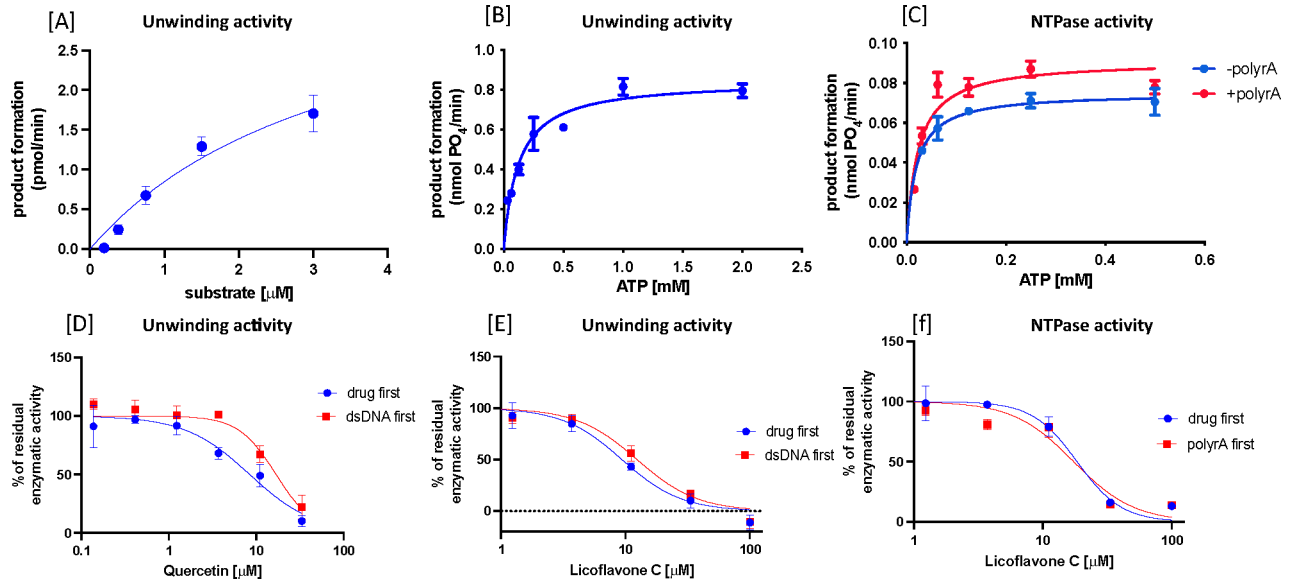


**Figure 5.** SARS-CoV-2 nsp13 kinetic parameters measured in the presence of BSA and TCEP and the impact of time of addition of nucleic acid on compound activity: [A] nsp13 unwinding-associated kinetics measured varying the DNA substrate; [B] nsp13 unwinding-associated kinetics measured varying the ATP substrate; [C] nsp13 ATPase-associated kinetics measured varying the ATP substrate (blue line) or the ATP substrate in the presence of ssRNA (red line); [D] inhibition of the nsp13-associated unwinding activity by quercetin preincubating nsp13 for 10 min with the dsDNA substrate (red line) or quercetin (blue line); [E] inhibition of the nsp13-associated unwinding activity by licoflavone C preincubating nsp13 for 10 min with the dsDNA substrate (red line) or licoflavone C (blue line); [F] inhibition of the nsp13-associated ATPase activity by licoflavone C preincubating nsp13 for 10 min with the dsDNA substrate (red line) or licoflavone C (blue line).

activity in the presence of BSA and TCEP (Figure S1). DNA unwinding enzyme kinetics showed an increase in the $k_{cat}$ value from 54.25 to 238.4 $min^{-1}$ in the absence or in the presence of BSA/TCEP, respectively, with a modest increase in the $K_m$ value for the dsDNA substrate, from 1.22 to 1.68 ± 0.60 mM, and for the ATP substrate, from 0.043 ± 0.012 to 0.122 ± 0.016 mM, in the absence or in the presence of BSA/TCEP, respectively (Figure 5). ATPase enzyme kinetics showed an increase of the $k_{cat}$ value from 211 to 2028 ± 36 $min^{-1}$ and no change in the $K_m$ value for the ATP substrate (from 0.043 ± 0.012 to 0.019 ± 0.009 mM), in the absence or in the presence of BSA/TCEP, respectively (Figure 5).

Second, the compounds that were able to inhibit the nsp13 unwinding activity were tested in these new assay conditions, observing a general decrease in their potency of inhibition: SSYA10−001 showed an $IC_{50}$ value of 1.73 μM, while quercetin was the most active natural compound ($IC_{50}$ = 6.8 μM) followed by licoflavone C ($IC_{50}$ = 9.9 μM) (Table 2). The same conditions were used to assay the effect of licoflavone C on the nps13 ATPase activity, and in this case, no significant variation in the $IC_{50}$ value was observed (29.0 ± 2.1 μM) with respect to the one previously measured (Table 2).

Next, we asked whether the time of addition of the nucleic acid in the reaction mixture could affect a compound's potency


https://doi.org/10.1021/acsptsci.1c00253
ACS Pharmacol. Transl. Sci. 2022, 5, 226−239

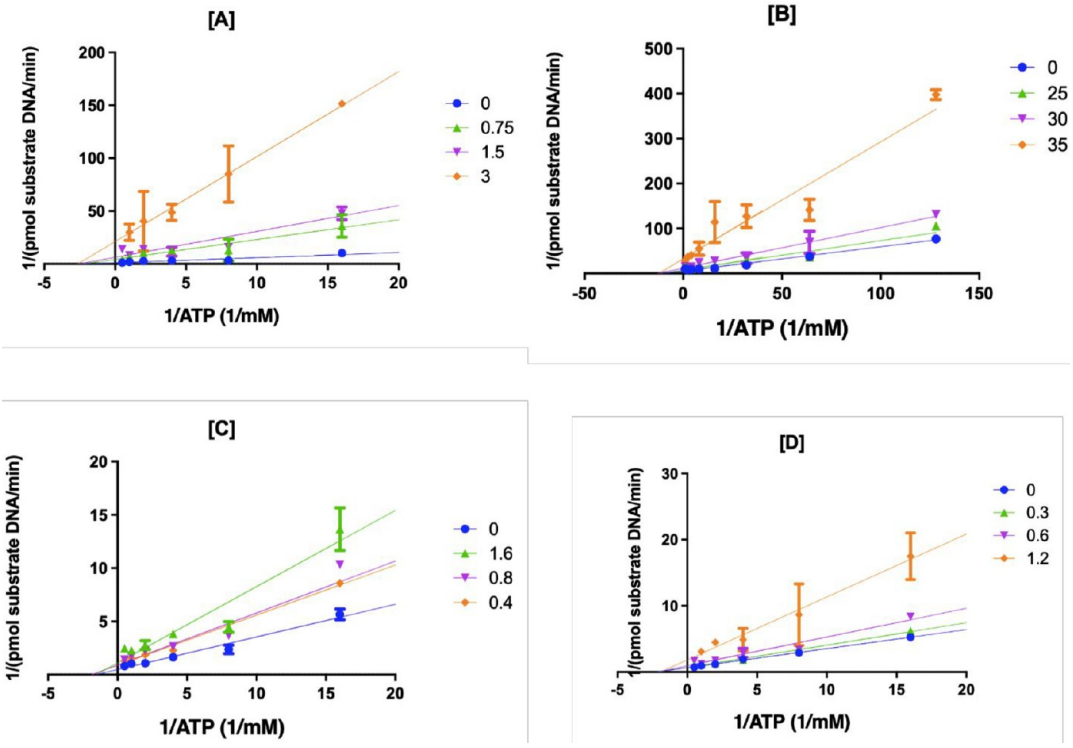


**Figure 6.** Kinetics of inhibition of nsp13-associated activities by flavonoids. [A] Inhibition of the nsp13-associated unwinding activity by licoflavone C; [B] inhibition of the ATPase activity by licoflavone C; [C] inhibition of the unwinding activity by kaempferol; [D] inhibition of the unwinding activity by flavanone.

of inhibition of the nsp13 unwinding assay. To this aim, nsp13 unwinding inhibition by quercetin and licoflavone C was measured by preincubating the enzyme for 10 min either with the nucleic acid or the drug, then the second component (drug or nucleic acid) was added, and the reaction was started by adding ATP (Figure 5D,E). Results showed that licoflavone C inhibition was not affected by preincubation of nsp13 with the nucleic acid, while quercetin inhibition was negatively affected with a 2-fold increase in the $IC_{50}$ value (from 8.4 to 16.9 $\mu$M). These results were in accordance with the higher affinity of quercetin for the dsRNA-binding site predicted by modeling calculations (Table 1).

Moreover, since CoV nsp13 ATPase activity has been previously detected also in the presence of circular plasmid DNA, reflecting the nsp13 ATPase activity during protein translocation on ssDNA,[25] we asked whether the presence of a nucleic acid could have an impact on the inhibition of the ATPase function by natural compounds using a poly(A) ssRNA of 350 base pairs. First, the impact of the presence of the poly(A) ssRNA on the nsp13 ATPase kinetics was evaluated (Figure 5C). Results showed that the presence of a poly(A) ssRNA positively affects nps13 ATPase activity, in accordance to what previously reported.[25] In fact, the $V_{max}$ value was increased with respect to the $V_{max}$ values measured in the absence of poly(A) RNA, with a consequent slight increase of the $k_{cat}$ value to 2487 $\pm$ 80 $min^{-1}$. Differently, the presence of poly(A) RNA had no impact on the ATP $K_m$ value (0.022 $\pm$ 0.004 mM). Next, all the compounds found to inhibit nsp13 unwinding activity were tested also in the presence of poly(A) RNA, and a further column was added to Table 1. Results showed that, also in these experimental conditions, only licoflavone C inhibited the nsp13 ATPase activity and that poly(A) RNA had only a slightly but not significant effect on the licoflavone C potency of inhibition ($IC_{50}$ = 18.3 $\pm$ 2.8 $\mu$M).

The nine most active flavonoids ($IC_{50}$ < 20 $\mu$M) were also tested on the SARS-CoV-2 replication in Vero E6-GFP cells using the compound GC376 as a positive control.[24] As Vero cells express at high levels the efflux transporter P-glycoprotein (P-gp), also known as MDR1 and ABCB1,[26] the SARS-CoV-2 replication assays were performed in the presence of 2 $\mu$M CP-100356, a P-gp efflux inhibitor.[27] Results showed that while GC376 inhibited SARS-CoV-2 replication with an $EC_{50}$ value of 2.9 $\mu$M, none of the tested flavonoids were able to inhibit viral replication, even though none of them were cytotoxic (Table 1).

**Determination of Flavonoid Kinetics of nsp13 Inhibition.** The obtained results, showing that flavanone, kaempferol, myricetin, and quercetin are able to inhibit only the nsp13-associated unwinding activity, while licoflavone C is able to inhibit both nsp13-associated functions, suggested that they might possess different modes of nsp13 inhibition. In addition, the fact that flavanone activity was affected by the presence of DTT also implied possible differences in its mode of action as compared with the other compounds. Hence, we wanted to investigate the kinetics of inhibition of nsp13 by these molecules. We first assessed the kinetics of inhibition of the nsp13-associated unwinding activity by licoflavone C, showing that it inhibited such nsp13 function noncompetitively versus ATP (Figure 6A). Second, we assessed the kinetics of inhibition by licoflavone C of the nsp13-associated ATPase activity, showing that its mode of action is noncompetitive also against this activity (Figure 6B). Third, we determined the kinetics of the inhibition of nsp13-associated unwinding activity by flavanone and kaempferol, observing that both compounds also inhibit this activity noncompetitively versus ATP (Figure 6C,D).



https://doi.org/10.1021/acsptsci.1c00253
ACS Pharmacol. Transl. Sci. 2022, 5, 226−239

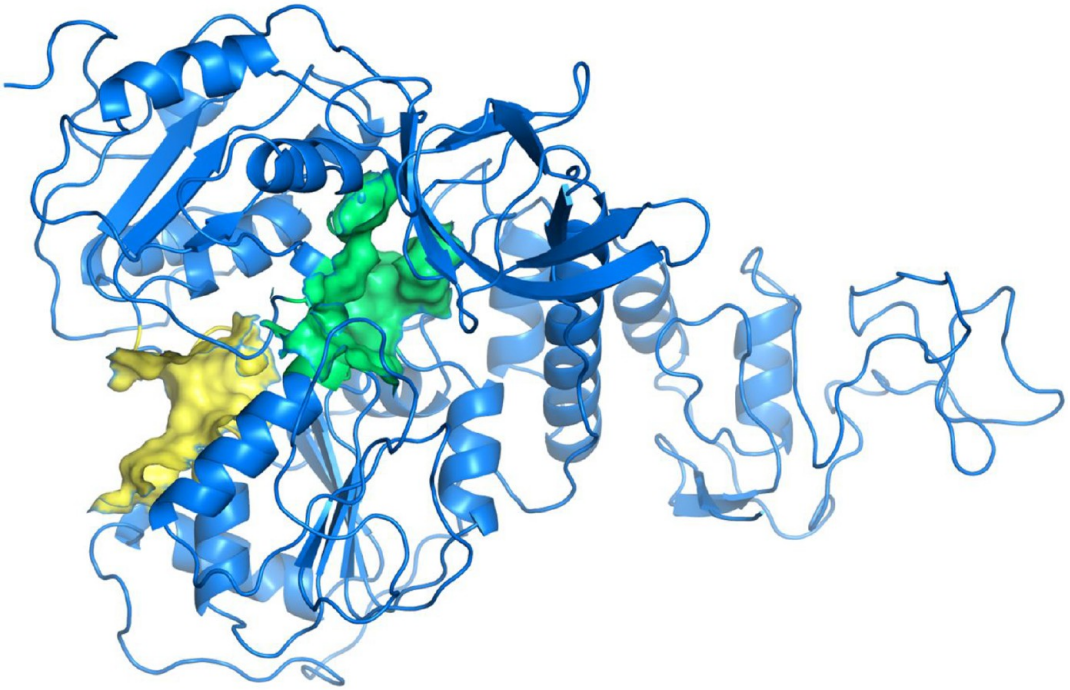

**Figure 7.** SARS-CoV-2 nsp13 NTP and 5′-RNA-binding sites. Nsp13 structure is shown as a blue cartoon and the NTP and 5′-RNA-binding sites are shown as yellow and green surfaces, respectively.

**Flavonoid Binding Mode Identification.** Given the obtained biochemical results, we wanted to further investigate the *in silico* interaction of the active compounds with nsp13. Hence, we first identified the nsp13 potential binding sites, using the nps13 chain from the cryo-electron microscopy structure of the nsp13-replication-transcription complex (Protein Data Bank ID: 6XEZ). Starting from this three-dimensional structure, we isolated the nsp13 helicase and identified two main binding sites: the nucleotide binding pocket (NTP site), occupied by ADP, and the 5′-RNA site (Figure 6), defined through a comprehensive mapping of the druggable cavities of nsp13; such an approach is implemented by the Pockets 2.0 plug-in for the VEGA ZZ suite of programs.[21] This site was also confirmed by the presence of the 5′-extension of the RNA template, in a subsequently published cryo-EM structure with PDB code 7CXM.[28] In support of our proposed model, we considered a crystallographic fragment screen against SARS-CoV-2 nsp13 helicase reported by by Newman and co-workers,[28] who deposited 52 crystal structures. Notably, in the NTP's site, there is much overlapping among the hydrophobic features of the described flavonoids and the cocrystallized probes.

Second, we investigated the interaction of the most representative ligands with these nsp13 binding sites, starting by examining the structural differences within the NTP site of licoflavone C, a flavone which has a 3-methylbut-2-enyl pendant on its scaffold, myricetin, which has the typical structure of a hydroxyflavone, flavanone, the representative of the flavanone class, and quercetin. Results showed that licoflavone C and myricetin share some key contact points with the amino acid residues Lys569, Gly538, and His290, which support their possible binding within the nsp13 NTP-binding site (Figure 8). Moreover, quercetin shows the Lys569 in common with licoflavone C and myricetin and two strong interactions with Glu540 and Ser289 (Figure 8D). Noteworthy, lycoflavone C was also shown to be able to interact with the amino acid residue Arg442, which is positioned in a loop that is not contacted by myricetin, thus expanding its range of interaction. In contrast, flavanone was not observed to establish direct interactions within the NTP pocket. Next, we evaluated the binding mode of the same ligands within the 5′-RNA site. Results showed that the three examined ligands share a key interaction with Arg560 and that licoflavone C was able to reach significantly deeper into the binding pocket and interact with the backbone of Cys309 (Figure 8). These important differences in the licoflavone C interactions observed in both binding sites could explain its experimentally observed ability to inhibit both nsp13-associated unwinding and ATPase activities and its high *in silico* affinity for both pockets.

## DISCUSSION

Despite the availability of a number of vaccines against SARS-CoV-2 infection, the inevitable development of new variants, the patient's conditions in which the vaccine are not effective, and the overall world pandemic situation urgently call for the development of SARS-CoV-2 direct antiviral agents. The viral nsp13 5′−3′ helicase is a validated drug target having two associated enzymatic functions: a nucleic acid unwinding activity and a NTPase activity. Given some previous reports on the effect of natural polyphenolic compounds on SARS-CoV functions,[17−19] our previous *in silico* studies[21] and that, at the best of our knowledge, there is a lack of data reported on nsp13 inhibitors,[20,29] we decided to perform an *in silico* analysis of a small natural compound library. Molecular docking studies showed a different theoretical affinity of the studied compounds with respect to the two identified NTP and 5′-RNA-binding sites indicating that, among them, licoflavone C has the highest predicted affinity for both sites while myricetin, baicalein, kaempferol, and quercetin have a good predicted affinity especially for 5′-RNA-binding site. Then, based on this analysis, we decided to assess the effect of a small in-house library of


https://doi.org/10.1021/acsptsci.1c00253
ACS Pharmacol. Transl. Sci. 2022, 5, 226−239

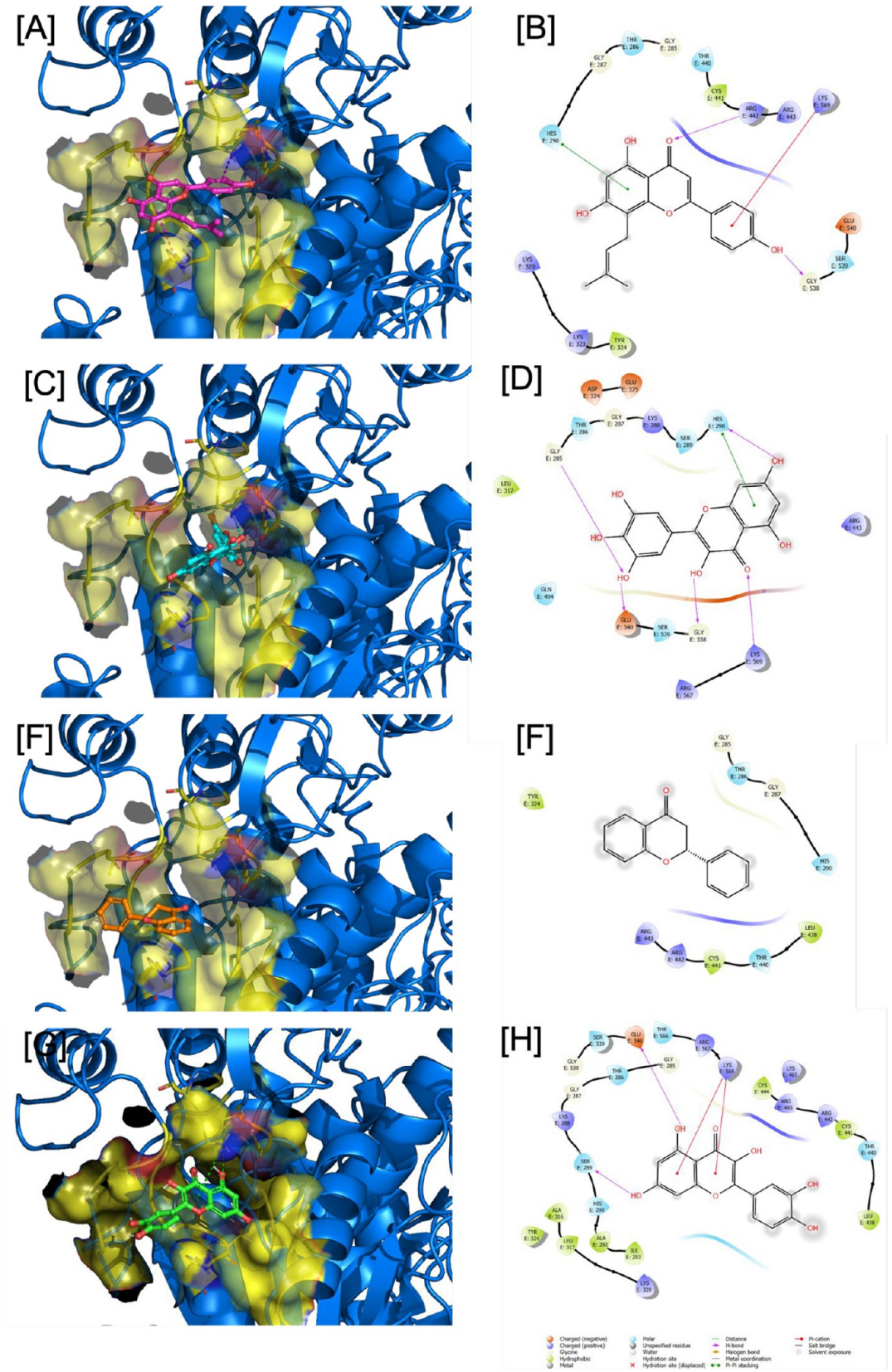


**Figure 8.** Binding of flavonoids to the nsp13 NTP-binding site. Representation of (A,B) licoflavone C (purple sticks), (C,D) myricetin (cyan sticks), (E,F) flavanone (orange sticks) and quercetin (green sticks) (G,H) binding mode. The Nsp13 3D structure is shown as a blue cartoon, the NTP-binding site is shown as a yellow surface, and the key residues are shown as sticks, 2D diagrams of compounds binding and their interactions with the corresponding pocket.



https://doi.org/10.1021/acsptsci.1c00253
*ACS Pharmacol. Transl. Sci.* 2022, 5, 226−239

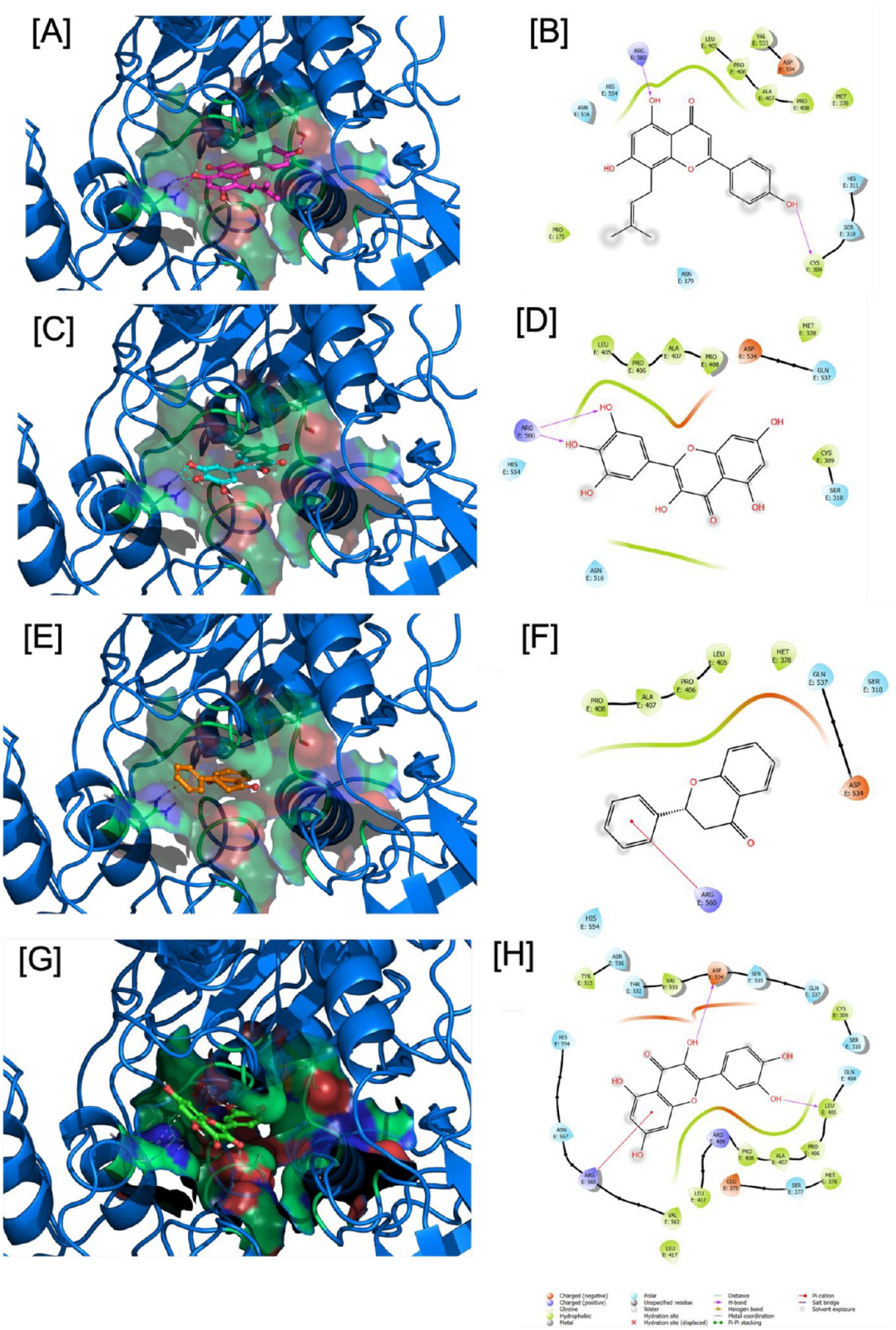


**Figure 9.** Binding of flavonoids to nsp13 5′-RNA-binding site. Representation of (A,B) licoflavone C (purple sticks), (C,D) myricetin (cyan sticks), (E,F) flavanone (orange sticks) and quercetin (green sticks) (G,H) binding mode. The Nsp13 3D structure is shown as a blue cartoon, the RNA-binding site is shown as a green surface, and the key residues are shown as sticks, 2D diagrams of compounds binding and their interactions with the corresponding pocket.

commercially available natural polyphenols, mostly flavonoids, on both SARS-CoV-2 nsp13-associated functions, expanding the number of chemical species evaluated *in silico* by testing also compounds bearing a glucoside moiety.



https://doi.org/10.1021/acsptsci.1c00253
*ACS Pharmacol. Transl. Sci.* 2022, 5, 226−239

We observed that out of the 21 tested compounds, only the flavonoids are able to inhibit the SARS-CoV-2 nsp13-associated unwinding activity with 11 derivatives showing $IC_{50}$ values below 30 $\mu$M. Results showed that nsp13 enzyme activities and flavonoids inhibition were affected by the presence of BSA and TCEP. On the one hand, the reduction of the flavonoids' potency of inhibition could be explained by their reported nonspecific binding to BSA.[30] On the other hand, however, the fact that the presence of BSA positively affects the enzyme catalytic performances, with variations in $k_{cat}$ and $K_m$ values indicating a direct effect of BSA on the enzyme, possibly modifying its conformation distributions. In this case, BSA might affect nsp13 conformation distributions and in turn the small molecule binding to nsp13. This second hypothesis seems to be supported by the observation that the licoflavone C potency of inhibition of the ATPase activity is not affected by the presence of BSA/TCEP, while its potency of inhibition of the unwinding activity shows a 9-fold decrease. We believe this could be an important aspect to be considered in designing and testing new nsp13 inhibitors. Compound SSYA10−001 was used as a positive control, showing that it is able to inhibit the SARS-CoV-2 nsp13-associated unwinding activity and does not block the ATPase activity, as previously reported for SARS-CoV.[31] Of note, SSYA10−001 showed similar activity on SARS-CoV-2 ($IC_{50}$ = 1.7 $\mu$M) to the one reported for SARS-CoV ($IC_{50}$ = 5.3 $\mu$M).[31]

Qualitative structure−activity relationships show that the most active compounds (kaempferol, myricetin, and quercetin) have 4−6 decorating hydroxyl substituents on the chromone core, while current data suggest that their position does not influence the compound potency of inhibition. Among tested compounds, the majority of the derivatives bearing the glucoside moiety was inactive on any of the two enzyme activities. The exception is the flavanone-7-O-glucoside molecule that inhibited the nsp13-associated unwinding activity with an $IC_{50}$ value of 2.8 $\mu$M. While the reason of this different behavior is not clear at the moment, it is worth noting that flavanone, the only tested molecule not decorated by hydroxyl groups, is also the only one whose inhibition was significantly affected by the presence of DTT, possibly suggesting that the oxidation state might alter either some nsp13 amino acid residues involved in its binding or the electron-rich ligand itself. Unfortunately, when tested on SARS-CoV-2 replication, none of the flavonoid derivatives were able to inhibit viral replication, partly in agreement with previous observations that flavonoids are often able to interact with viral proteins and inhibit some enzyme activities but rarely inhibit viral replication.[32−34]

SARS-CoV and SARS-CoV-2 nsp13 proteins share a very high sequence homology; however, present results on the effect of flavonoids on SARS-CoV-2 nsp13 differ from the ones previously published on SARS-CoV nsp13.[17−19] In fact, in the previously published screening of >60 flavonoid derivatives on SARS-CoV nsp13, none inhibited the nsp13-associated unwinding activity, but a few inhibited the ATPase-associated functions.[17,18] Among the reported compounds, myricetin and baicalein were the flavonoids we studied on SARS-CoV-2 nsp13 whose effects on SARS-CoV nsp13 were already reported. Nsp13 unwinding assay conditions in which the compounds were tested differed for oligonucleotide length and overhang, while the ATPase assay condition differed for the presence or not of ssDNA, but whether these assay differences are causing different assay behaviors is not clear at the moment.

Considering the different abilities of the tested compounds to inhibit the two SARS-CoV-2 nsp13-associated enzyme functions, it is worth noting that the two biochemical assays we used to assess the two enzymatic functions have an intrinsic difference: the unwinding assays measure the opening of a short double-strand nucleic acid due to the nsp13 movement along the substrate oligonucleotide, while the ATPase assay measures the production of Pi. Hence, the two assays imply a different level of protein dynamics. The first readout, in fact, requires a protein translocation along a nucleic acid that lacks to the second. For this reason, we wanted to test the nsp13-assocated ATPase activity also in the presence of a poly(A) RNA that should allow such protein translocation dynamics, showing that the presence of the ssRNA, although enhancing enzyme activity in accordance to what was previously reported,[25] does not alter the licoflavone C ability to inhibit such protein function. Furthermore, when tested on nsp13 unwinding activity, the binding of nps13 to the substrate dsDNA before licoflavone C addition does not affect the licoflavone C potency inhibition, suggesting a strong protein−inhibitor interaction that is not displaced by substrate binding. Differently, the quercetin potency of inhibition of the nsp13 unwinding activity was negatively affected by the previous nsp13 binding to DNA, in accordance with the higher affinity of quercetin for the dsRNA-binding site predicted by modeling calculations.

Based on the results obtained and to acquire a further piece of information on the binding of the active compounds on nsp13, we performed kinetics of inhibition studies on flavanone, kaempferol, and licoflavone C, showing that all compounds are noncompetitive inhibitors with respect to the ATP substrate. In particular, licoflavone C is a noncompetitive inhibitor of both nsp13-associated functions. Noncompetitive kinetics was also observed for the SSYA10−001 inhibition of the SARS-CoV nsp13 unwinding activity.[31]

Altogether, the noncompetitive nature of the nsp13 inhibition shown by the tested compounds and the performed docking studies suggest that the active compounds bind to the same binding sites but with significant differences. To further comment on this hypothesis, we superimposed licoflavone C, myricetin, quercetin, and flavanone fitting into both nsp13 binding sites, suggesting that there are differences in the key interaction between the nsp13 amino acid residues and myricetin and flavanone, on the one side, and licoflavone C on the other side (Figure 9). In particular, licoflavone C, the only flavonoid bearing an alkyl substituent in position 8 and the one predicted as the best in the ranking capable of fitting well in both bonding sites, is shown to have a unique pattern of protein interaction, entering much deeper in the binding sites, and of enzyme inhibition. Hence, it is possible to speculate that such differences are responsible for the different effects of the compounds on nsp13 activities, even though further studies will be required to dissect the biological effects of such interactions.

In conclusion, we have established biochemical assays for both nsp13-associated enzyme activities and screened *in silico* and *in vitro* a small in-house library of natural compounds, reporting for the first time the ability of some flavonoids to inhibit the enzymatic activities of SARS-CoV-2 nsp13, a validated drug target, in the low micromolar range. We showed that compounds act noncompetitively against ATP on both nsp13-associated activities and that they can fit both NTP- and RNA-binding sites of nsp13. Among the tested compounds, only licoflavone C, which has a unique pattern of interaction with nsp13 amino acid residues, was shown to inhibit both nsp13-


https://doi.org/10.1021/acsptsci.1c00253
ACS Pharmacol. Transl. Sci. 2022, 5, 226−239

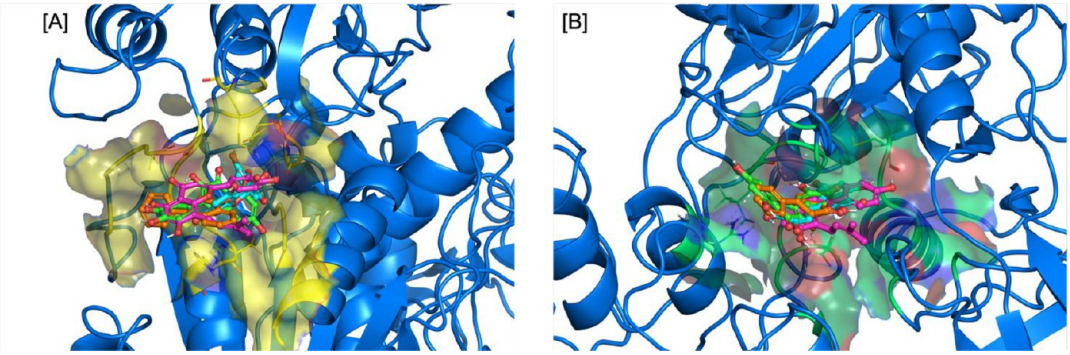


**Figure 10.** Compounds binding to nsp13. Representation of the licoflavone C (purple sticks), myricetin (cyan sticks), quercetin (green sticks), and flavanone (orange sticks) binding modes in both binding sites. The Nsp13 helicase 3D structure is shown as a blue cartoon, and the nucleotide- and 5′-RNA-binding sites are shown as yellow (A) and green (B) surfaces, respectively.

associated enzyme activities, not altered by substrate binding. Although the studied compounds were not able to block viral replication, and therefore are not suitable to be used as drugs, further development and exploration of the interaction of studied compounds and nsp13 can lead to novel, more potent derivatives inhibiting both enzyme activities and viral replication.

## MATERIALS AND METHODS

**Compounds.** All compounds were commercially available and >95% pure by HPLC analysis.

**SARS-CoV-2 nsp13 Expression and Purification.** SARS-CoV-2 nsp13 was expressed from pNIC-ZB vector in Rosetta cells, using TB medium for culture, according to Newman et al.[28] For the first step of purification, a HisTrap column was used, and eluted fractions were further purified on a HiTrap SP column. After overnight digestion with TEV protease, sample was loaded onto a HiLoad 16/600 Superdex pg column. The final yield of purification was around 3 mg of pure protein from 4 L of culture.

**Determination of SARS-CoV-2 nsp13 Unwinding-Associated Activity.** The SARS-CoV-2 nsp13 unwinding-associated activity was measured in black 384-well plates (PerkinElmer), in 40 $\mu$L of reaction volume containing 20 mM Tris−HCl, pH 7.2, 50 mM NaCl, 2 $\mu$M Hel Capture oligo (5′-TGG TGC TCG AAC AGT GAC-3′) from Biomers, 5 mM $MgCl_2$, 5% DMSO or inhibitor, and 1 nM purified nsp13. The reaction mixture containing the enzyme was preincubated for 10 min with inhibitor at room temperature (RT). The reaction was started by adding 1 mM ATP and 750 nM annealed DNA substrate (5′-AGT CTT CTC CTG GTG CTC GAA CAG TGA C-Cy3-3′, 5′-BHQ-2-GTC ACT GTT CGA GCA CCA CCT CTT CTG A-3′) from Biomers. After 15 min of incubation at 37 °C, products were measured with Victor Nivo (Perkin) at 530/580 nm.

**Determination of SARS-CoV-2 nsp13 ATPase-Associated Activity.** The SARS-CoV-2 nsp13 helicase-associated activity was measured in a transparent 96-well plate (PerkinElmer), in 25 $\mu$L of reaction volume containing 20 mM Tris−HCl, pH 7.2, 50 mM NaCl, 2 mM $MgCl_2$, 5% DMSO or inhibitor, and 25 nM purified nsp13, with or without 10 $\mu$g/mL of BSA and 180 $\mu$M TCEP. The reaction was started by adding 400 $\mu$M ATP. After 30 min of incubation at 37 °C, 50 $\mu$L of Biomol Green Reagent (Prod. No. BML-AK111, Enzo Lifescience) was added, and the reaction was incubated for 10 min at RT, protected from the light. Products were measured with Victor Nivo (Perkin) at 650 nm.

**Kinetics of SARS-CoV-2 nsp13 Unwinding-Associated Activity with Respect to the DNA Substrate.** The SARS-CoV-2 nsp13 unwinding-associated activity was measured in 40 $\mu$L of reaction volume containing 20 mM Tris−HCl, pH 7.2, 50 mM NaCl, 2 $\mu$M Hel Capture oligo (5′-TGG TGC TCG AAC AGT GAC-3′), 5 mM $MgCl_2$, 5% DMSO (or compound), and 1 nM purified nsp13, with or without 10 $\mu$g/mL of BSA and 180 $\mu$M TCEP. The reaction mixture containing the enzyme was preincubated for 10 min with inhibitor at RT, and then, increasing concentrations of annealed DNA substrate (5′-AGT CTT CTC CTG GTG CTC GAA CAG TGA C-Cy3-3′, 5′-BHQ-2-GTC ACT GTT CGA GCA CCA CCT CTT CTG A-3′) were added. The reaction was started by adding 1 mM final ATP. After 15 min of incubation at 37 °C, products were measured with Victor Nivo (Perkin) at 530/580 nm. Processed product was quantified by interpolation of a standard curve of free Cy3-labeled oligonucleotide obtained by Biomers.

**Kinetics of SARS-CoV-2 nsp13 Unwinding-Associated Activity with Respect to the ATP Substrate.** The SARS-CoV-2 nsp13 unwinding-associated activity was measured in 40 $\mu$L of reaction volume containing 20 mM Tris−HCl, pH 7.2, 50 mM NaCl, 2 $\mu$M Hel Capture oligo (5′-TGG TGC TCG AAC AGT GAC-3′) (Biomers), 5 mM $MgCl_2$, 5% DMSO (or compound), and 1 nM purified nsp13, with or without 10 $\mu$g/mL of BSA and 180 $\mu$M TCEP. The reaction mixture containing the enzyme was preincubated for 10 min with inhibitor at RT. Then, 750 nM DNA substrate (5′-AGT CTT CTC CTG GTG CTC GAA CAG TGA C-Cy3-3′, 5′-BHQ-2-GTC ACT GTT CGA GCA CCA CCT CTT CTG A-3′) (Biomers) was added, and the reaction was started adding increasing concentrations of ATP. After 15 min of incubation at 37 °C, products were measured with Victor Nivo (Perkin) at 530/580 nm.

**Kinetics of SARS-CoV-2 nsp13 ATPase-Associated Activity with Respect to the ATP Substrate.** The SARS-CoV-2 nsp13 ATPase-associated activity was measured in 25 $\mu$L of reaction volume containing 20 mM Tris−HCl, pH 7.2, 50 mM NaCl, 2 mM $MgCl_2$, 5% DMSO or different concentrations of inhibitor, and 25 nM purified nsp13, with or without 10 $\mu$g/mL of BSA, 180 $\mu$M TCEP, and 0.75 $\mu$M 350-base-pair poly(A)RNA. The reaction was started by adding increasing concentrations of ATP. After 30 min of incubation at 37 °C, 50 $\mu$L of Biomol Green Solution (Enzo Lifescience) was added, and the reaction was incubated for 10 min at RT, protected from the light. Products were measured with Victor Nivo (Perkin) at 650


https://doi.org/10.1021/acsptsci.1c00253
ACS Pharmacol. Transl. Sci. 2022, 5, 226−239

nm. The amount of phosphate generated was quantified by interpolation of a phosphate standard curve (Prod. No. BML-KI102, Enzo Lifescience).

**Data Analysis.** Data analysis of assay development results was performed using GraphPad Prism Version 9.1.2. Test compound results were normalized relative to respective controls. Dose response curves were fitted to a nonlinear regression of (log10)dose vs normalized response-variable slope. Assay quality was assessed using the $Z'$-factor calculation with $Z' > 0.5$ as the threshold for acceptance.

**SARS-CoV-2 Replication Assay.** The African green monkey kidney cell line, previously engineered to constitutively express GFP (Vero E6-GFP), was kindly provided by Janssen Pharmaceutical. Cells were maintained in Dulbecco's modified Eagle's medium (DMEM; Gibco) supplemented with 10% v/v fetal beef serum (FBS; Gibco), 0.075% sodium bicarbonate (7.5% solution, Gibco), and 1× Pen-strep (Euroclone) and kept under 5% $CO_2$ on 37 °C. SARS-CoV-2 strain BetaCov/Belgium/GHB-03021/2020 was provided by KU Leuven. All virus-related work was carried out in certified, high-containment biosafety level-3 facilities at the University of Cagliari. Cells were seeded at 10 000 cells/well in 96-well plates. The following day, cells were incubated with the control compounds and the virus at different MOI 0.01. GC376 compound[24] was used as positive control, in the presence of 2 $\mu$M p-gp inhibitor CP-100356.[26] The media was removed 72 h post infection, and the total well GFP fluorescence was measured with a Victor 3 with 485/535 nm excitation wavelength. The inhibition of viral replication was calculated as the percentage of the viral induced cytopathic effect on infected untreated controls.

**Evaluation of Cytotoxicity.** Vero E6-GFP cells were seeded at 10 000 cells/well in 96-well plates; the following day, cells were incubated with the compounds, and 72 h post infection, the media was removed, and the total well GFP fluorescence was measured with a Victor 3 with a 485/535 nm excitation wavelength. The cytotoxicity was calculated as the percentage of fluorescence of untreated controls.

**3D Structure Models and Virtual Screening Protocol LiGen.** The crystal structures of the SARS-CoV-2 nsp13 were obtained from the Protein Data Bank (pdb code: 6XEZ) and prepared by removing water solvents and crystallization additives. The hydrogen atoms were added by using the VEGA program[35] to remain compatible with physiological pH. The protein structure was then minimized using NAMD2[36] to avoid geometrical clashes and by keeping the backbone atoms fixed to preserve the resolved folding but optimizing the lateral chains. The geometrical docking procedure implemented in LiGen, a proprietary software developed by Dompé, was used for the docking simulations.[37] The analyzed molecules were classified with high, medium, and low theoretical affinity, based on their ability to correctly accommodate the binding site and on their capability to establish specific chemical interactions with the residues of the binding site.

In order to setup computational studies, ligands were converted to 3D and prepared with Schrödinger's LigPrep tool.[38] This process generated for each ligand multiple stereoisomers, tautomers, ring conformations (one stable ring conformer by default), and protonation states. Another Schrödinger package, Epik,[39] was used to select tautomers and protonation states that would be dominant at a selected pH range (pH = 7 ± 1). Ambiguous chiral centers were enumerated, allowing a maximum of 32 isomers to be produced from each input ligand structure. Then, an energy minimization was performed with the OPLS3 force field on all the 3D candidate ligands.

## ■ ASSOCIATED CONTENT

### Supporting Information

The Supporting Information is available free of charge at https://pubs.acs.org/doi/10.1021/acsptsci.1c00253.

Figure S1. SARS-CoV-2 nsp13 activities in different reaction mixtures; Figure S2. enlarged version of Figure 6 (PDF)

## ■ AUTHOR INFORMATION


### Corresponding Author

**Enzo Tramontano** − *Dipartimento di Scienze della vita e dell'ambiente, Università degli Studi di Cagliari, Cittadella Universitaria di Monserrato, 09042 Cagliari, Italy;* orcid.org/0000-0002-4849-0980; Email: tramon@unica.it

### Authors

**Angela Corona** − *Dipartimento di Scienze della vita e dell'ambiente, Università degli Studi di Cagliari, Cittadella Universitaria di Monserrato, 09042 Cagliari, Italy;* orcid.org/0000-0002-6630-8636

**Krzysztof Wycisk** − *Laboratory of Protein Structure, International Institute of Molecular and Cell Biology, Warsaw 02-109, Poland*

**Carmine Talarico** − *Dompé Farmaceutici SpA, 67100 L'Aquila, Italy*

**Candida Manelfi** − *Dompé Farmaceutici SpA, 67100 L'Aquila, Italy*

**Jessica Milia** − *Dipartimento di Scienze della vita e dell'ambiente, Università degli Studi di Cagliari, Cittadella Universitaria di Monserrato, 09042 Cagliari, Italy*

**Rolando Cannalire** − *Department of Pharmacy, University of Napoli "Federico II", Napoli 80131, Italy*

**Francesca Esposito** − *Dipartimento di Scienze della vita e dell'ambiente, Università degli Studi di Cagliari, Cittadella Universitaria di Monserrato, 09042 Cagliari, Italy*

**Philip Gribbon** − *Fraunhofer Institute for Translational Medicine and Pharmacology (ITMP), 22525 Hamburg, Germany; Fraunhofer Cluster of Excellence for Immune Mediated Diseases (CIMD), 60590 Frankfurt, Germany*

**Andrea Zaliani** − *Fraunhofer Institute for Translational Medicine and Pharmacology (ITMP), 22525 Hamburg, Germany; Fraunhofer Cluster of Excellence for Immune Mediated Diseases (CIMD), 60590 Frankfurt, Germany*

**Daniela Iaconis** − *Dompé Farmaceutici SpA, 67100 L'Aquila, Italy*

**Andrea R. Beccari** − *Dompé Farmaceutici SpA, 67100 L'Aquila, Italy*

**Vincenzo Summa** − *Department of Pharmacy, University of Napoli "Federico II", Napoli 80131, Italy;* orcid.org/0000-0002-6288-2681

**Marcin Nowotny** − *Laboratory of Protein Structure, International Institute of Molecular and Cell Biology, Warsaw 02-109, Poland;* orcid.org/0000-0001-8632-0977

Complete contact information is available at: https://pubs.acs.org/10.1021/acsptsci.1c00253


### Notes

The authors declare no competing financial interest.



https://doi.org/10.1021/acsptsci.1c00253
ACS Pharmacol. Transl. Sci. 2022, 5, 226−239

## ■ ACKNOWLEDGMENTS

This work was supported by Exscalate4Cov under the European Union's Horizon 2020 research and innovation program under grant agreement No 101003551. The authors thank Janssen Pharmaceutical for providing the African green monkey kidney cell line that was engineered to constitutively express GFP (Vero E6-GFP) and the Pieter Leyssen laboratory of KU Leuven for providing the SARS-CoV-2 strain BetaCov/Belgium/GHB-03021/2020. R.C. acknowledges MIUR-Ministero dell'Istruzione, dell'Università e della Ricerca (Italian Ministry of Education, University and Research), PON R&I 2014-2020-AIM (Attraction and International Mobility), project AIM1873131 - Num. Attività 2 - Linea 2.1.

## ■ ABBREVIATIONS

RdRp, RNA-dependent RNA polymerase; nsp, nonstructural protein; NTPase, nucleotidyl phosphatase

## ■ REFERENCES

(1) Chen, N.; Zhou, M.; Dong, X.; Qu, J.; Gong, F.; Han, Y.; Qiu, Y.; Wang, J.; Liu, Y.; Wei, Y.; Xia, J.; Yu, T.; Zhang, X.; Zhang, L. Epidemiological and Clinical Characteristics of 99 Cases of 2019 Novel Coronavirus Pneumonia in Wuhan, China: A Descriptive Study. *Lancet (London, England)* **2020**, *395* (10223), 507−513.

(2) Wu, F.; Zhao, S.; Yu, B.; Chen, Y. M.; Wang, W.; Song, Z. G.; Hu, Y.; Tao, Z. W.; Tian, J. H.; Pei, Y. Y.; Yuan, M. L.; Zhang, Y. L.; Dai, F. H.; Liu, Y.; Wang, Q. M.; Zheng, J. J.; Xu, L.; Holmes, E. C.; Zhang, Y. Z. A New Coronavirus Associated with Human Respiratory Disease in China. *Nature* **2020**, *579* (7798), 265−269.

(3) Zhou, P.; Yang, X.-L.; Wang, X. G.; Hu, B.; Zhang, L.; Zhang, W.; Si, H. R.; Zhu, Y.; Li, B.; Huang, C. L.; Chen, H. D.; Chen, J.; Luo, Y.; Guo, H.; Jiang, R. Di; Liu, M. Q.; Chen, Y.; Shen, X. R.; Wang, X.; Zheng, X. S.; Zhao, K.; Chen, Q. J.; Deng, F.; Liu, L. L.; Yan, B.; Zhan, F. X.; Wang, Y. Y.; Xiao, G. F.; Shi, Z. L. A Pneumonia Outbreak Associated with a New Coronavirus of Probable Bat Origin. *Nature* **2020**, *579* (7798), 270−273.

(4) Tvarogová, J.; Madhugiri, R.; Bylapudi, G.; Ferguson, L. J.; Karl, N.; Ziebuhr, J. Identification and Characterization of a Human Coronavirus 229E Nonstructural Protein 8-Associated RNA 3′-Terminal Adenylyltransferase Activity. *J. Virol.* **2019**, *93* (12), 291−310.

(5) Gao, Y.; Yan, L.; Huang, Y.; Liu, F.; Zhao, Y.; Cao, L.; Wang, T.; Sun, Q.; Ming, Z.; Zhang, L.; Ge, J.; Zheng, L.; Zhang, Y.; Wang, H.; Zhu, Y.; Zhu, C.; Hu, T.; Hua, T.; Zhang, B.; Yang, X.; Li, J.; Yang, H.; Liu, Z.; Xu, W.; Guddat, L. W.; Wang, Q.; Lou, Z.; Rao, Z. Structure of the RNA-Dependent RNA Polymerase from COVID-19 Virus. *Science* **2020**, *368* (6492), 779−782.

(6) Snijder, E. J.; Decroly, E.; Ziebuhr, J. The Nonstructural Proteins Directing Coronavirus RNA Synthesis and Processing. *Adv. Virus Res.* **2016**, *96*, 59−126.

(7) V'kovski, P.; Kratzel, A.; Steiner, S.; Stalder, H.; Thiel, V. Coronavirus Biology and Replication: Implications for SARS-CoV-2. *Nat. Rev. Microbiol.* **2021**, *19*, 155.

(8) Lehmann, K. C.; Snijder, E. J.; Posthuma, C. C.; Gorbalenya, A. E. What We Know but Do Not Understand about Nidovirus Helicases. *Virus Res.* **2015**, *202*, 12−32.

(9) Adedeji, A. O.; Marchand, B.; Te Velthuis, A. J. W.; Snijder, E. J.; Weiss, S.; Eoff, R. L.; Singh, K.; Sarafianos, S. G. Mechanism of Nucleic Acid Unwinding by SARS-CoV Helicase. *PLoS One* **2012**, *7* (5), e36521.

(10) Saikrishnan, K.; Powell, B.; Cook, N. J.; Webb, M. R.; Wigley, D. B. Mechanistic Basis of 5′-3′ Translocation in SF1B Helicases. *Cell* **2009**, *137* (5), 849−859.

(11) Singleton, M. R.; Dillingham, M. S.; Wigley, D. B. Structure and Mechanism of Helicases and Nucleic Acid Translocases. *Annual Review of Biochemistry. Annu. Rev. Biochem* **2007**, *76*, 23−50.

(12) Hao, W.; Wojdyla, J. A.; Zhao, R.; Han, R.; Das, R.; Zlatev, I.; Manoharan, M.; Wang, M.; Cui, S. Crystal Structure of Middle East Respiratory Syndrome Coronavirus Helicase. *PLoS Pathog.* **2017**, *13* (6), e1006474.

(13) Jia, Z.; Yan, L.; Ren, Z.; Wu, L.; Wang, J.; Guo, J.; Zheng, L.; Ming, Z.; Zhang, L.; Lou, Z.; Rao, Z. Delicate Structural Coordination of the Severe Acute Respiratory Syndrome Coronavirus Nsp13 upon ATP Hydrolysis. *Nucleic Acids Res.* **2019**, *47* (12), 6538−6550.

(14) Chen, J.; Malone, B.; Llewellyn, E.; Grasso, M.; Shelton, P. M. M.; Olinares, P. D. B.; Maruthi, K.; Eng, E. T.; Vatandaslar, H.; Chait, B. T.; Kapoor, T. M.; Darst, S. A.; Campbell, E. A. Structural Basis for Helicase-Polymerase Coupling in the SARS-CoV-2 Replication-Transcription Complex. *Cell* **2020**, *182* (6), 1560−1573.e13.

(15) van Dinten, L. C.; van Tol, H.; Gorbalenya, A. E.; Snijder, E. J. The Predicted Metal-Binding Region of the Arterivirus Helicase Protein Is Involved in Subgenomic MRNA Synthesis, Genome Replication, and Virion Biogenesis. *J. Virol.* **2000**, *74* (11), 5213−5223.

(16) Zhang, R.; Li, Y.; Cowley, T. J.; Steinbrenner, A. D.; Phillips, J. M.; Yount, B. L.; Baric, R. S.; Weiss, S. R. The Nsp1, Nsp13, and M Proteins Contribute to the Hepatotropism of Murine Coronavirus JHM.WU. *J. Virol.* **2015**, *89* (7), 3598−3609.

(17) Keum, Y.; Jeong, Y. Development of Chemical Inhibitors of the SARS Coronavirus: Viral Helicase as a Potential Target. *Biochem. Pharmacol.* **2012**, *84* (10), 1351−1358.

(18) Yu, M. S.; Lee, J.; Lee, J. M.; Kim, Y.; Chin, Y. W.; Jee, J. G.; Keum, Y. S.; Jeong, Y. J. Identification of Myricetin and Scutellarein as Novel Chemical Inhibitors of the SARS Coronavirus Helicase, NsP13. *Bioorg. Med. Chem. Lett.* **2012**, *22* (12), 4049−4054.

(19) Keum, Y. S.; Lee, J. M.; Yu, M. S.; Chin, Y. W.; Jeong, Y. J. Inhibition of SARS Coronavirus Helicase by Baicalein. *Bull. Korean Chem. Soc.* **2013**, *34* (11), 3187−3188.

(20) White, M. A.; Lin, W.; Cheng, X. Discovery of COVID-19 Inhibitors Targeting the SARS-CoV-2 Nsp13 Helicase. *J. Phys. Chem. Lett.* **2020**, *11*, 9144−9151.

(21) Gervasoni, S.; Vistoli, G.; Talarico, C.; Manelfi, C.; Beccari, A. R.; Studer, G.; Tauriello, G.; Waterhouse, A. M.; Schwede, T.; Pedretti, A. A Comprehensive Mapping of the Druggable Cavities within the SARS-CoV-2 Therapeutically Relevant Proteins by Combining Pocket and Docking Searches as Implemented in Pockets 2.0. *Int. J. Mol. Sci.* **2020**, *21* (14), 5152.

(22) Lee, N. R.; Kwon, H. M.; Park, K.; Oh, S.; Jeong, Y. J.; Kim, D. E. Cooperative Translocation Enhances the Unwinding of Duplex DNA by SARS Coronavirus Helicase NsP13. *Nucleic Acids Res.* **2010**, *38* (21), 7626−7636.

(23) Adedeji, A. O.; Singh, K.; Calcaterra, N. E.; DeDiego, M. L.; Enjuanes, L.; Weiss, S.; Sarafianos, S. G. Severe Acute Respiratory Syndrome Coronavirus Replication Inhibitor That Interferes with the Nucleic Acid Unwinding of the Viral Helicase. *Antimicrob. Agents Chemother.* **2012**, *56* (9), 4718−4728.

(24) Kuzikov, M.; Costanzi, E.; Reinshagen, J.; Esposito, F.; Vangeel, L.; Wolf, M.; Ellinger, B.; Claussen, C.; Geisslinger, G.; Corona, A.; Iaconis, D.; Talarico, C.; Manelfi, C.; Cannalire, R.; Rossetti, G.; Gossen, J.; Albani, S.; Musiani, F.; Herzog, K.; Ye, Y.; Giabbai, B.; Demitri, N.; Jochmans, D.; Jonghe, S.; Rymenants, J.; Summa, V.; Tramontano, E.; Beccari, A. R.; Leyssen, P.; Storici, P.; Neyts, J.; Gribbon, P.; Zaliani, A. Identification of Inhibitors of SARS-CoV-2 3CL-Pro Enzymatic Activity Using a Small Molecule in Vitro Repurposing Screen. *ACS Pharmacol. Transl. Sci.* **2021**, *4*, 1096.

(25) Tanner, J. A.; Watt, R. M.; Chai, Y. B.; Lu, L. Y.; Lin, M. C.; Peiris, J. S. M.; Poon, L. L. M.; Kung, H. F.; Huang, J. D. The Severe Acute Respiratory Syndrome (SARS) Coronavirus NTPasefhelicase Belongs to a Distinct Class of 5′ to 3′ Viral Helicases. *J. Biol. Chem.* **2003**, *278* (41), 39578−39582.

(26) Hu, Y.; Ma, C.; Szeto, T.; Hurst, B.; Tarbet, B.; Wang, J. Boceprevir, Calpain Inhibitors II and XII, and GC-376 Have Broad-Spectrum Antiviral Activity against Coronaviruses. *ACS Infect. Dis.* **2021**, *7* (3), 586−597.

(27) De Rosa, M. F.; Sillence, D.; Ackerley, C.; Lingwood, C. Role of Multiple Drug Resistance Protein 1 in Neutral but Not Acidic

Glycosphingolipid Biosynthesis. *J. Biol. Chem.* **2004**, *279* (9), 7867−7876.
(28) Newman, J. A.; Douangamath, A.; Yadzani, S.; Yosaatmadja, Y.; Aimon, A.; Brandão-Neto, J.; Dunnett, L.; Gorrie-stone, T.; Skyner, R.; Fearon, D.; Schapira, M.; von Delft, F.; Gileadi, O. Structure, Mechanism and Crystallographic Fragment Screening of the SARS-CoV-2 NSP13 Helicase. *Nat. Commun.* **2021**, *12* (1), 1−11.
(29) Zeng, J.; Weissmann, F.; Bertolin, A. P.; Posse, V.; Canal, B.; Ulferts, R.; Wu, M.; Harvey, R.; Hussain, S.; Milligan, J. C.; Roustan, C.; Borg, A.; McCoy, L.; Drury, L. S.; Kjaer, S.; McCauley, J.; Howell, M.; Beale, R.; Diffley, J. F. X. Identifying SARS-CoV-2 Antiviral Compounds by Screening for Small Molecule Inhibitors of Nsp13 Helicase. *Biochem. J.* **2021**, *478* (13), 2405−2423.
(30) Liu, S.; Guo, C.; Guo, Y.; Yu, H.; Sun, M. Z.; Greenaway, F. Comparative Binding Affinities of Flavonoid Phytochemicals with Bovine Serum Albumin. *Iran. J. Pharm. Res. IJPR* **2014**, *13* (3), 1019.
(31) Adedeji, A. O.; Marchand, B.; te Velthuis, A. J. W.; Snijder, E. J.; Weiss, S.; Eoff, R. L.; Singh, K.; Sarafianos, S. G. Mechanism of Nucleic Acid Unwinding by SARS-CoV Helicase. *PLoS ONE* **2012**, *7* (5), e36521.
(32) Daino, G. L.; Frau, A.; Sanna, C.; Rigano, D.; Distinto, S.; Madau, V.; Esposito, F.; Fanunza, E.; Bianco, G.; Taglialatela-Scafati, O.; Zinzula, L.; Maccioni, E.; Corona, A.; Tramontano, E. Identification of Myricetin as an Ebola Virus VP35-Double-Stranded RNA Interaction Inhibitor through a Novel Fluorescence-Based Assay. *Biochemistry* **2018**, *57* (44), 6367−6378.
(33) Sanna, C.; Rigano, D.; Corona, A.; Piano, D.; Formisano, C.; Farci, D.; Franzini, G.; Ballero, M.; Chianese, G.; Tramontano, E.; Taglialatela-Scafati, O.; Esposito, F. Dual HIV-1 Reverse Transcriptase and Integrase Inhibitors from Limonium Morisianum Arrigoni, an Endemic Species of Sardinia (Italy). *Natural Product Research.* **2019**, *33*, 1798−1803.
(34) Fanunza, E.; Iampietro, M.; Distinto, S.; Corona, A.; Quartu, M.; Maccioni, E.; Horvat, B.; Tramontano, E. Quercetin Blocks Ebola Virus Infection by Counteracting the VP24 Interferon Inhibitory Function. *Antimicrob. Agents Chemother.* **2020**, *64* (7), e00530-20.
(35) Pedretti, A.; Mazzolari, A.; Gervasoni, S.; Fumagalli, L.; Vistoli, G. The VEGA Suite of Programs: An Versatile Platform for Cheminformatics and Drug Design Projects. *Bioinformatics* **2021**, *37* (8), 1174−1175.
(36) Phillips, J. C.; Hardy, D. J.; Maia, J. D. C.; Stone, J. E.; Ribeiro, J. V.; Bernardi, R. C.; Buch, R.; Fiorin, G.; Hénin, J.; Jiang, W.; McGreevy, R.; Melo, M. C. R.; Radak, B. K.; Skeel, R. D.; Singharoy, A.; Wang, Y.; Roux, B.; Aksimentiev, A.; Luthey-Schulten, Z.; Kalé, L. V.; Schulten, K.; Chipot, C.; Tajkhorshid, E. Scalable Molecular Dynamics on CPU and GPU Architectures with NAMD. *J. Chem. Phys.* **2020**, *153* (4), No. 044130.
(37) Manelfi, C.; Gossen, J.; Gervasoni, S.; Talarico, C.; Albani, S.; Philipp, B. J.; Musiani, F.; Vistoli, G.; Rossetti, G.; Beccari, A. R.; Pedretti, A. Combining Different Docking Engines and Consensus Strategies to Design and Validate Optimized Virtual Screening Protocols for the SARS-CoV-2 3CL Protease. *Mol. 2021, Vol. 26, Page 797* **2021**, *26* (4), 797.
(38) Dixon, S. L.; Duan, J.; Smith, E.; Von Bargen, C. D.; Sherman, W.; Repasky, M. P. AutoQSAR: An Automated Machine Learning Tool for Best-Practice Quantitative Structure-Activity Relationship Modeling. *Future Med. Chem.* **2016**, *8* (15), 1825−1839.
(39) Shelley, J. C.; Cholleti, A.; Frye, L. L.; Greenwood, J. R.; Timlin, M. R.; Uchimaya, M. Epik: A Software Program for PKa Prediction and Protonation State Generation for Drug-like Molecules. *J. Comput. Aided. Mol. Des.* **2007**, *21* (12), 681−691.


https://doi.org/10.1021/acsptsci.1c00253
*ACS Pharmacol. Transl. Sci.* 2022, 5, 226−239